Nd$_{2X}$Cd$_{2-3X}$SiO$_4$ (0.01≤X≤0.21) 고용체의 합성과 구조 규명

S. Ramesh* and B. B. Das

Department of Chemistry, School of Physical, Chemical and Applied Sciences, Pondicherry University,
Pondicherry, India-605014
(접수 2010. 7. 20; 수정 2010. 12. 16; 게재확정 2011. 4. 5)

Synthesis, Structure and Characterization of Nd$_{2X}$Cd$_{2-3X}$SiO$_4$ (0.01≤X≤0.21) Solid-Solutions

S. Ramesh* and B. B. Das

Department of Chemistry, School of Physical, Chemical and Applied Sciences, Pondicherry University,
*Pondicherry, India-605014. *Email: rameshsiva_chem@yahoo.com*
(Received July 20, 2010; Revised December 16, 2010; Accepted April 5, 2011)

요 약. Nd$_{2x}$Cd$_{2-3x}$SiO$_4$ (0.01≤x≤0.21) [S1-S3: x=0.01, 0.11 and 0.21] 고용체를 졸-겔 방법을 통해 합성하였다. X선 분말 회절(XRD) 측정은 P2$_1$/m 공간군의 단사정계를 보여준다. 평균 결정 크기는 20-45 nm이다. 주사전자현미경(SEM)으로 살펴본 모양은 구형의 특성을 보인다. 에너지 분산 X 선 분광기(EDS) 결과로부터 모든 구성 원소의 존재를 확인하였다. ~750 nm에서의 흡수 밴드는 Nd^{3+} 이온의 ^{4}I$_{9/2}$→^{4}F$_{7/2}$+^{4}S$_{3/2}$ 전이에 기인한다. 10, 40, 77, 300 K에서 S1-S3의 전자 상자성 공명 (EPR) 선모양은 Nd^{3+} 이온의 빠른 스핀 격자 이완에 기인하는 폭이 넓은 구분되지 않은 등방성의 선모양을 보여준다.

주제어: 나노복합재료, 졸-겔, X선 회절, 광학 특성, 전자 상자성 공명

ABSTRACT. Synthesis of Nd$_{2x}$Cd$_{2-3x}$SiO$_4$ (0.01≤x≤0.21) [S1-S3: x=0.01, 0.11 and 0.21] solid solutions were prepared by sol-gel method. Powder x-ray diffraction (XRD) results show monoclinic unit cell with space group P2$_1$/m. The average crystallite sizes are found to be 20 to 45 nm. The Scanning Electron Microcopy (SEM) images show morphology of the sample is in globular nature. The energy dispersive analysis of x-rays (EDX) and X-ray mapping results confirmed that all the constituent elements of the composites were present and that were distributed in uniformly. The optical absorption band at ~750 nm was due to ^{4}I$_{9/2}$→^{4}F$_{7/2}$+^{4}S$_{3/2}$ transition optically active Nd^{3+} ions. Electron Paramagnetic Resonance (EPR) lineshapes of S1-S3 at 10, 40, 77 and 300 K show a broad unresolved isotropic lineshapes were observed due to rapid spin lattice relaxation of Nd^{3+}.

Keywords: Nanocomposites, Sol-gel, X-ray diffraction, Optical properties, Electron paramagnetic resonance

INTRODUCTION

The characteristics of silica-based rare-earth materials are of particular interest for optical applications especially important in Optical fiber technology where rare-earth doped Transition Metal (TM) silicates are needed to create nonreciprocal devices such as isolators and circulators and magnetic field sensors. Indeed these compositions also shows the characteristics in the visible and infrared optical lasers, amplifiers, photonics, up-conversion luminescence for applications such as color displays,[1,2] high density optical data reading and storage.[3,4] Superconductor,[5,6] magnetic materials,[7,8] medical[9] and etc, due to the extremely high melting points of rare-earth oxides and SiO.

Recently, chemists pay more attention on Pr^{3+}, Nd^{3+}, Sm^{3+} and Er^{3+} doped Transition Metal (TM) compounds because these materials can be used in the visible spectral region at room temperature. Considering the high coordination number of RE^{3+} may render the structural flexibility and increase the stability of the RE^{3+} doped Transition Metal (TM) composites. The Nd^{3+} doped silicates for optical lasers in the visible region have not been studied in detail. There are only a few investigations about the electronic structures and spectroscopic parameters of Nd^{3+} in crystals and glasses.[10-13]

The host materials are very important factor for developing rare-earth-doped optical devices. The researchers have concentrated on oxides and silicates are more suitable for practical applications because of their high chemical durability and thermal stabilities. Silicates are one of the most popular crystal hosts for making optical fiber

lasers and amplifiers due to the nontoxic silica is an ideal network forming material because of its capability to form extensive cross linking network. However, the characterization of the materials is more essential to the systematic devolvement of the new materials synthesis and understanding how they behave in practical applications. The sol-gel method provides an approach to obtain rare-earth silicates as pure homogeneous materials at much lower temperatures and processing time required by conventional techniques.

In this report, we discuss our method of sol-gel synthesis and structure-property relations in a series of similar Nd-doped Cadmium silicate nanocrystalline powder using varieties of direct and indirect structure-sensitive solid state techniques.

EXPERIMENTAL

Syntheses of Nd$_{2x}$Cd$_{2-3x}$SiO$_4$ (0.01≤x≤0.21) nano-composites

Various techniques are available for the preparation of nanomaterials. They include dividing or breaking down of bulk solids. Some of the very well known methods are laser ablation, vapor deposition, plasma synthesis and high energy milling. All these technique involve special condition, equipment and high temperature. The authors prepared Nd$_{2x}$Cd$_{2-3x}$SiO$_4$ (0.01≤x≤0.21) solid solution by employing the sol-gel method. Sol-gel technique offers an excellent control over the stoichiometry and allows lower processing temperature, and easier to introduce of dopants it leads to produce multi-component oxide powder at the nanoscale.[14,15] In this method we already prepared Cu$_x$Na$_{4-2x}$SiO$_4$ using TEOS as the starting materials.
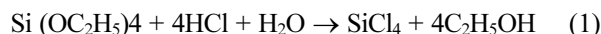
Analytical grade chemicals were used to prepare the Nd$_{2x}$Cd$_{2-3x}$SiO$_4$ (0.01≤x≤0.21) solid solution. In all the cases tetraethoxysilane (TEOS: Si (OC$_2$H$_5$)$_4$), cadmium acetate (Cd (CH$_3$COO)$_2$) and neodymium acetate (Nd (CH$_3$COO)$_3$) were used with stoichiometric amounts. The types and the amounts of starting materials were varied to obtain the chemical compositions shown in *Table* 1.

The calculated amounts of ethonalic solutions of tetraethoxysilane (TEOS) were prepared. The reaction mechanism as follows in equation 1.

$$Si (OC_2H_5)4 + 4HCl + H_2O \rightarrow SiCl_4 + 4C_2H_5OH \quad (1)$$

To the above solution calculated amount of finely powered cadmium acetate were added followed by 20 ml of 1-Propanol and 2-Butanol were added to get the clear solution then the mixture was stirred in a magnetic stirrer for 1 h. To the resulting silica sol, calculated amount of finely powdered neodymium acetate was added and temperature of the solution was maintained at 50 °C and it was allowed to stir for 72 hours. Into the Nd-doped sol if necessary supplementary ethanol (ETOH) was added until the solution would become homogeneous. To the Nd-doped sol 20 ml of cyclohexane is added and then liquid ammonia is added to control the pH (pH~7) of the solution in order to get the transparent gel. The resulting gel is broken by heating about 120 °C and fine powder is obtained. The powder is then heated in a high temperature furnace at 850 °C for 4 h and quenched in air to obtain the Nd-doped cadmium silicate nanosize powder. The pictorial representation of the preparation methods is shown in *Fig*. 1.

Characterizations

The room temperature X-ray powder diffraction patterns of the Nd$_{2x}$Cd$_{2-3x}$SiO$_4$ (0.01≤x≤0.21) solid solutions were collected on a PANalytical X'Pert Pro diffractometer in Bragg-Brentano configuration using monochromatic Co K radiation (Cu Kα 1, 2 (λ ~ 1.54060, 1.54443A), equipped with a Gobel mirror, a Braun PSD detector and operating at 40 kV-30 mA in the range 2θ = 5-80° with a 2θ step size of 0.02°. Rietveld refinements were carried out with the program FullProf[16,17] (Windows version, October 2009) using the pseudo-Voigt profile function of Thompson *et al.*.[18]

Table 1. The calculated amount of starting chemicals of the Nd$_{2x}$Cd$_{2-3x}$SiO$_4$ (0.01≤x≤0.21) (S1-S3) solid solutions

Sample code	Nd(CH$_3$COO)$_3$ (g)	Cd(CH$_3$COO)$_2$ (g)	Si(OC$_2$H$_5$)$_4$ (ml)
S1	0.0868	7.0971	3.0181
S2	0.9763	6.1466	3.0835
S3	1.9052	5.1541	3.1517

Tetraethoxysilane +Hydrochloric acid → Tetrachlorosilane

⇩ **1 hour**

[Cd(CH3COO)2]

⇩

20ml of 1-propanol & 2-butanol

⇩ **1 hour stirring**

Nd (CH3COO)2

pH~7 ⇩ **72 hours stirring, heating at ~50^{0}C**

The pours materials are obtained

⇩ **Sintering at 850^{0}C**

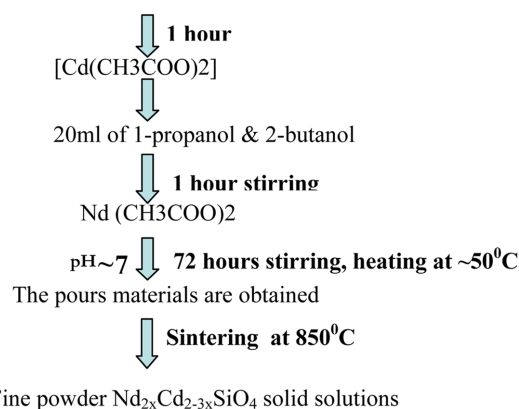Fine powder Nd$_{2x}$Cd$_{2-3x}$SiO$_4$ solid solutions

Fig. 1. Sol Synthetic method of Nd$_{2x}$Cd$_{2-3x}$SiO$_4$ (0.01≤x≤0.21) solid-solutions.

The background was refined by adjusting the height of pre-selected points for linear interpolation. The experimental density (d_E) of the samples was determined by liquid displacement method and theoretical density (d_T) were calculated by x-ray analysis. Surface morphology, elemental analysis and elemental mapping studies were carried out using a Scanning Electron Microscope (SEM) (Hitachi-S3400) equipped with Energy Dispersive Analysis of X-rays (EDAX) (Super dryer-II). The Differential scanning calorimetric (DSC) traces of Samples S1-S5 was done in a Universal V2.6D TA Instruments in the range 50-613 ºC. The DSC trace of the sample shows an endothermic change.

The IR spectrum of the glasses was recorded at room temperature in the range 400-4000 cm^{-1} by ABB BOMEM FTIR-104 spectrometer using "KBr pellet technique. The optical absorption spectra of the samples were recorded on a Varian Spectrophotometer (Model Carry 5000 D) in the range 200-800 nm in the solid phase. The EPR experiments at 10 K, 40 K, and at 300 K were performed at X-band on a Varian E-122 spectrometer. Samples were run at low temperatures using an Air Products Helitran cryostat. The magnetic field was calibrated using with a Varian NMR Gauss meter and frequency meter were used to record the line shapes in these cases, a g-standard is not necessary. The g-factors can be computed directly from the spectra using the recorded value of the frequency and the field position. X-band ESR spectral measurement at 77 K were done with a JEOL JES-TE 100 ESR spectrometer system with 100 kHz field modulation and a phase sensitive detector to obtain first derivative signal. Quartz sample tubes were used for recording the EPR spectra of powder specimens. In order to measure the line width variation as a function of composition in the samples the line shapes were recorded with sufficiently low microwave power to avoid saturation. The magnetic field calibration have been made with respect to the resonance line of DPPH (g_{DPPH} = 2.00354) which is used as a field marker.

RESULTS AND DISCUSSION

Fig. 2 shows the powder X-ray diffraction patterns of the $Nd_{2x}Cd_{2-3x}SiO_4$ ($0.01 \leq x \leq 0.21$) nanocomposites. The obtained powder samples were single phase as determined by XRD. Further structural information was obtained by the careful Rietveld refinements analysis with the FullProf program using the pseudo-Voigt profile function of Thompson *et al*. The XRD patterns were entirely indexed for all the samples. It shows that samples were formed in monoclinic lattice type with $P2_1/m$ space group. The unit cell volumes of the samples were increasing with the composition of x. The calculated lattice parameters of the samples are given in the *Table* 2.

The average crystallite sizes of the samples were calculated by Debye-Scherrer formula[19] and Williamson-Hall plot[20] are shown as follows (1) and (2) respectively.

$$D = K\lambda / \beta \cos\theta \qquad (1)$$
$$B\cos\theta = K\lambda / D + 2\,\varepsilon\,\sin\theta \qquad (2)$$

Where D- crystallite size, K= Scherrer constant, λ represents the wavelength of Cu Kα radiation, β stands for the corrected half width of the diffraction peak, θ is the Bragg angle of the X-ray diffraction peak and ε is the lattice strain. The gaussion function gives a better fit to the FWHM of all the patterns then the lorentzian function.

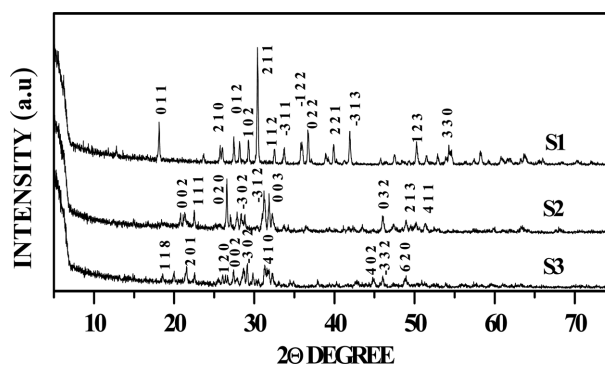*Fig.* 2. Powder x-ray diffraction pattern of the $Nd_{2x}Cd_{2-3x}SiO_4$ ($0.01 \leq x \leq 0.21$).

Table 2. Lattice parameters and space group of the $Nd_{2x}Cd_{2-3x}SiO_4$ ($0.01 \leq x \leq 0.21$) (S1-S3) solid solutions

Sample code	S1	S2	S3
Lattice type	Monoclinic	Monoclinic	Monoclinic
a (Aº)	8.7469 ± 0.0029	9.5267 ± 0.0025	13.1506 ± 0.0031
b (Aº)	6.4386 ± 0.0021	6.7131 ± 0.0026	7.0197 ± 0.0026
c (Aº)	8.0238 ± 0.0018	9.4233 ± 0.0015	6.8405 ± 0.0031
β	110.31 ± 0.0027	117.99 ± 0.0034	108.02 ± 0.0052
Unit cell volume	423.78	532.14	600.50
Z	4	4	4

Table 3. Average crystallite sizes, density and porosity of the of the Nd$_{2x}$Cd$_{2-3x}$SiO$_4$ (0.01≤x≤0.21) (S1-S3) solid solutions

S. No	Average crystallite sizes (nm)		Density (gcm^{-3})		Porosity, P (%)
	Scherrer	Willkinson-Hall	Calculated	Experimental	
S1	40.183	45.320	3.91	3.36	14.06
S2	25.865	24.900	3.94	3.28	16.75
S3	25.628	20.572	3.39	2.81	17.11

Therefore, the observed XRD patterns are essentially gaussion, pointing to the uniform crystallite size distribution. The estimated average crystallite sizes are 45 nm (S1), 24 nm (S2) and 20 nm (S3). The sizes of the particles were decreased from S1-S3 which is due to the increases of Nd^{3+} and decreases of cd^{2+} ions. The porosity (p in percentage) of the samples was determined from X-ray density and experimental density by using the following expression:[21]

$$P = 1 - (d_E / d_x) \times 100 \qquad (3)$$

It is interesting that the porosity of the samples is increased as the concentration of the Nd^{3+} ion is increased. The values of crystallite sizes, experimental density, X-ray density and porosity of the samples are reported in *Table* 3.

The morphology of the samples S1-S3 is shown in *Fig.* 3(a). It shows that the particles are regular in globular nature and no other distinct changes in over the composition range (0.01≤x≤0.21) are shown. The interaction of grain boundary and porosity is important to determining the limited grain size. When many pores are present and the sintering temperature is not so high the grain growth is inhibited, particle can be obtained. The average grain size of the particle is bellow 50 nm which is slightly larger than the determined one by XRD. EDX profile and quantitative result was used to confirm the purity of the sample and the composition of the sample S3 is shown in the *Fig.* 3(b). It was observed that the obtained quantitative result of the sample S3 to be the similar as that of the expected composition range. The X-ray mapping of sample S3 shows that all the constituent elements were present and it is distributed uniformly. It is shown in the *Fig.* 3(c).

The DSC traces of the samples in the range 50-613 °C do not show any significant phase transformation of the studied composition range (S1-S3: x=0.01, 0.11 and 0.21). The IR spectra at 300 K of S1-S5 shows the presence of tetrahedral [SiO$_{4/2}$]$^{2-}$(symmetric bending[22]: 527 cm^{-1}; asymmetric stretch[23]: 1110 cm^{-1}) and [CdO$_{4/2}$]$^{2-}$ (symmetric stretch[24]: 556 cm^{-1}; asymmetric stretch[24]: 836-886 cm^{-1}) units.

The optical absorption spectra of Nd^{3+} in Nd$_{2x}$Cd$_{2-3x}$SiO$_4$
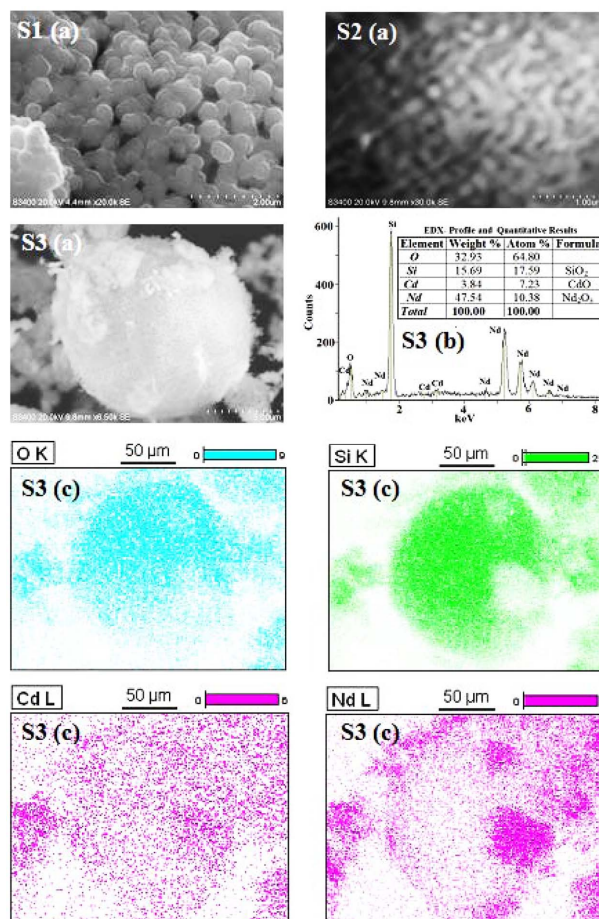

Fig. 3. (a) The SEM morphology of S1-S3, (b) EDX- profile of S3 and (c) X-ray mapping of S3 of the Nd$_{2x}$Cd$_{2-3x}$SiO$_4$ (0.01≤x ≤0.21).

(0.01≤x≤0.21) solid solutions were recorded in UV-Visible (200-800 nm) region and the wavelength of the observed bands along with their assignments were shown in *Fig.* 4. In the absorption spectrum, the strong absorption bands occur at near 357, 429, 474, 525, 580, 679, 740, 745, 750 790 and 800 nm. As well known, the rare earth atoms have the conguration 1s^{2}2s^{2}2p^{6}3s^2 3p^{6}3d^{10}4s^2 5s^{2}5p^{6}4f^n 5d^{1}6s^2 (n = 1-14), the trivalent RE^{3+} ions in solids lose all the 5d and 6s electrons. Since the optically active 4f electrons are shielded by the outer shell electrons, the 4f electrons of RE^{3+} ions are not strongly affected. In consequence, they produce only small energy splitting,
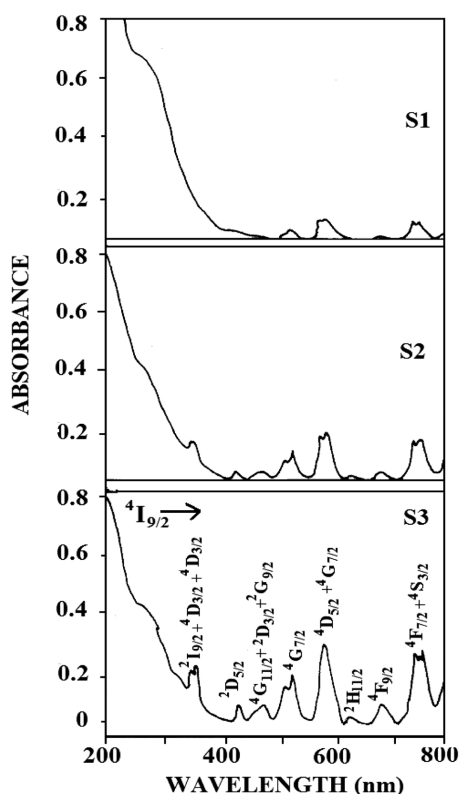
Fig. 4. The room temperature optical spectra of sample S1-S3 of the $Nd_{2x}Cd_{2-3x}SiO_4$ (0.01≤x≤0.21).

and the gross features of the energy level diagram of RE^{3+} ions are unchanged. Then, the assignments of RE^{3+} ion

transition from the ground state to excited states can be determined by comparison with the energy levels of RE^{3+} ions which were calculated by Carnall *et al.*.[25] Therefore, the absorption lines at 357, 429, 474, 525, 580, 679, 740, 745 and 800 are due to $4f^3$ - $4f^3$ transition of optically active Nd^{3+} ions.[26] The peak at ~750 nm is due to $^4I_{9/2}$ →$^4F_{7/2}$ + $^4S_{3/2}$ transition of Nd^{3+} ion.[27] The absorption peek at ~790 of $^4I_{9/2}$→$^4F_{5/2}$ transition is due to the electron level of $^4F_{5/2}$ relaxes to the $^4F_{3/2}$ electron level. This electron relaxation process expected to Nd^{3+} ions.[28] The above absorption peeks are commonly used for optical pumping of neodymium based lasers.[27] It is suggested that it may be regarded as a potential solid-state laser material for diode-laser pumped due to $4f^3$ - $4f^3$ transition of optically active Nd^{3+} ions.

Fig. 5(a), (b) and (c) shows that the EPR lineshapes of S1-S3 at 10, 77 and 300 K respectively. In *Fig.* 4(a) shows that the observed EPR lineshapes of S1 - S3 at 10 K along with simulated one of S1. The free ion of Nd^{3+} ($4f^3$) is having $^4I_{9/2}$ ground state, in a crystal field of D_{2d} symmetry $^4I_{9/2}$ splits up into five, Kramer's doublets, 9/2, 7/2, 5/2, 3/2, 1/2. Only the lowest doublet is populated at below 4 K. Therefore, the system can be described by a pseudo spin S=1/2. Nd has three even isotopes with I=0 and total natural abundances of 79.5%, and two isotopes[143] or [145]Nd (I=7/2) of natural abundances 12.2% and 8.3%, respectively. Therefore, the EPR spectrum of Nd^{3+} is expected to be composed of an intense central line due to the even iso-
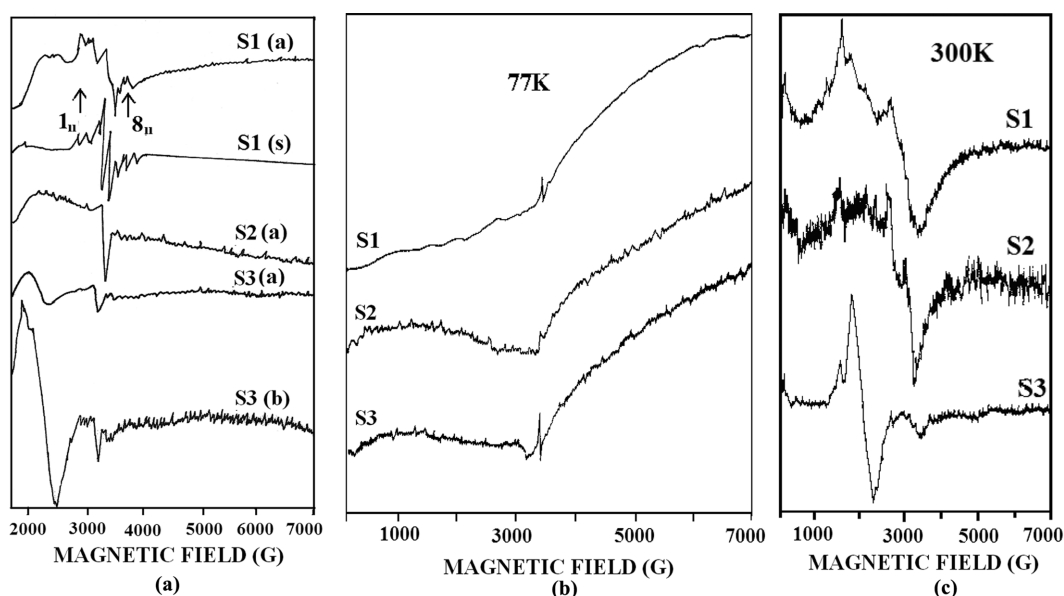

Fig. 5. (a) The EPR lineshapes of sample S1-S3 of the $Nd_{2x}Cd_{2-3x}SiO_4$ (0.01≤x≤0.21) at (a) 10 K, (b) 40 K and (s) simulation. (b) The EPR lineshapes of sample S1-S3 of the $Nd_{2x}Cd_{2-3x}SiO_4$ (0.01≤x≤0.21) at 77 K. (c) The EPR lineshapes of sample S1-S3 of the $Nd_{2x}Cd_{2-3x}SiO_4$ (0.01≤x≤0.21) at 300 K.

***Table* 4.** Observed EPR Spin Hamiltonian parameter of S1-S3 of Nd$_{2x}$Cd$_{2-3x}$SiO$_4$ (0.01≤x≤0.21) at 10, 40, 77 and 300 K

S. No.	Temp (K)	g$_∥$	g$_⊥$	g$_{iso}$	A$_∥$(G)	A$_⊥$(G)
S1	10	2.557	2.102	2.283	160	25
	77	-	-	1.992	-	-
	300	-	-	2.057	-	-
S2	10	-	-	2.046	-	-
	77	-	-	2.017	-	-
	300	-	-	2.054	-	-
S3	10	-	-	2.046	-	-
	40	-	-	2.022	-	-
	77	-	-	2.036	-	-
	300	-	-	1.974	-	-

topes and a hyperfine pattern with two sets of 2I+1=8 lines for the two odd isotopes.[29] So, the only EPR signal at 10 K of S1 (x=0.01) shows axially symmetric feature with 8-parallel lines with indication of doublet feature and unresolved perpendicular lines. The values of the spin Hamiltonian parameters of S1 is g$_∥$=2.557, g$_⊥$=2.102 (g$_{iso}$= 2.283), A$_∥$=160 G and A$_⊥$=25G obtained from simulation using Bruker's program simfonia. The sample S2 and S3 shows isotropic lineshapes at 10 K with same g$_{iso}$ values as 2.046. The calculated spin Hamiltonian parameters of the samples are listed in the *Table* 4. Further due to lowest level occupancy the lineshapes of S1-S3 at 77 (*Fig.* 4(b)) and 300 K (*Fig.* 4(c)) show only broad lines without any observable g-values due to rapid spin-lattice relaxation[30] of Nd^{3+} ions.

CONCLUSION

The synthesis and structural properties of Nd$_{2x}$Cd$_{2-3x}$SiO$_4$ (0.01≤x≤0.21solid solutions, with size between 20 and 45 nm were prepared using a sol gel method. From the XRD and DTA-TGA data, we observe that all the samples have only a single phase, monoclinic lattice type with P2$_1$/m space group. The morphology of the samples is in globular nature. The absorption band at ~790 of ^{4}I$_{9/2}$→^{4}F$_{5/2}$ transition is due to the electron level of ^{4}F$_{5/2}$ relaxes to the ^{4}F$_{3/2}$ electron level of Nd^{3+} ions, therefore these spectral characterizations of Nd^{3+} in Nd$_{2x}$Cd$_{2-3x}$SiO$_4$ nanocomposites suggest that it may be regarded as a potential solid-state laser material for diode laser pumping. The broad and unresolved EPR lineshapes of Nd^{3+} in the composites is due to the rapid spin-lattice relaxation. All the above are discussed in detail.

REFERENCES

1. McFarlane, R. A. *J. Opt. Soc. Am. B* **1994**, *11*, 871.
2. Maas, H.; Currao, A.; Calzaferri, G. *Angew. Chem. Int. Ed.* **2002**, *41*, 2495.
3. Brede, R.; Danger, T.; Heumann, E.; Huber, G.; Chai, B. *Appl. Phys. Lett.* **1993**, *63*, 729.
4. Lande, D.; Orlov, S. S.; Akella, A.; Hesselink, L.; Neurgaonkar, R. R. *Opt. Lett.* **1997**, *22*, 1722.
5. Aygun, G.; Atanassova, E.; Turan, R.; Babeva, Tz. *Mater. Chem. Phys.* **2005**, *89*, 316.
6. Chen, H.; Chen, X.; Li, X.; Hou, Y.; Wang, S.; Ren, Z.; Bai, J. *Opt. Laser. Tech.* **2009**, *41*, 1.
7. Shandong, L.; Hong, B.; Guozhi, X.; Zhonga, W.; Zhang, F.; Benxi, G.; Zhanga, J.; Lu, M.; Youwei, D. *Jour. Magn Magn. Materi.* **2004**, *282*, 202.
8. Liu, W.; Zhang, Z. D.; Liu, J. P.; Sun, X. K. *J. Appl. Phys.* **2000**, *87*, 5332.
9. Boxem, T. V. *Muller. Chest.* **1999**, *116*, 1108.
10. Zhao, B.; Cheng, P.; Dai, Y.; Cheng, C.; Liao, D. Z.; Yan, S. P.; Jiang, Z. H.; Wang, G. L. *Angew. Chem. Int. Ed.* **2003**, *42*, 934.
11. Sanada, T.; Suzuki, T.; Yoshida, T.; Kaizaki, S. *Inorg. Chem.* **1998**, *37*, 4712.
12. Li, Y. T.; Yan, C. W.; Zhang, J. *Cryst. Growth. Des.* **2003**, *3*, 481.
13. Liang, Y. C.; Hong, M. C.; Su, W.; Cao, R.; Zhang, W. J. *Inorg. Chem.* **2001**, *40*, 4574.
14. Zaghete, M. A.; Paivasantos, C. O.; Varela, J. A.; Lango, E.; Mascarenhas, Y. P. *J. Am. Ceram. Soc.* **1992**, *75*, 2088.
15. Cao, W.; Cross, L. E. *Phys. Rev. B* **1993**, *47*, 4825.
16. Rodríguez, C. J. *Physica B* **1993**, *192*, 55.
17. Rodríguez, C. J. *CPD Newsletter* **2001**, *26*, 12.
18. Thompson, P.; Cox, D. E.; Hastings, J. B. *J. Appl. Crys.* **1987**, *20*, 79.
19. Lin, W.; Ruixin, M.; Shao, W.; Liu, B. *Appl. Surf. Sci*, **2007**, *253*, 5179.
20. Williamson, G. K.; Hall, W. H. *Acta. Metall.* **1953**, *1*, 22.
21. Hankare, P. P.; Vader, V. T.; Patil, N. M.; Jadhav, S. D.; Sankpal, U. B.; Kadam, M. R.; Chougule, B. K.; Gajbhiye, N. S. *Mater. Chem. Phys.* **2009**, *113*, 233238.
22. Nakamoto, K. Infrared and Raman Spectra of Inorganic and Coordination Compounds, John Wiley and Sons, N.Y., **1986**: p.138.
23. Williams, Q. Mineral Physics and Crystallography, AGU, Reference shelf 2, p.291.
24. Reference 18, p. 133.
25. Carnall, W. T.; Goodman, G. L.; Rajnak, K.; Rana, R. S. *J. Chem. Phys.* **1989**, *90*, 3443.
26. Hu, Z. *J. Sol. State Chem.* **2004**, *177*, 3028.

27. Dharaj, K. *Polym. Int*. **2004**, *959*, 8103.
28. Honma, T.; Kusatsugu, M.; Komatsu, T. *Mater. Chem. Phys*. **2009**, *113*, 124129.
29. Guillot-Noel, O.; Simons, D.; Gourier, D. *J. Phys. Chem. Solids*. **1999**, *60*, 555.

30. Allenspach, P.; Mesot, J.; Staub, U.; Guillaume, M.; Kramer, M.; McCallum, R. W.; Maletta, H.; Blank, M. H.; Osborn, R.; Arai, M.; Bowden, Z. Taylor. *Z. Phys*. **1994**, *B95*, 301.